JACS
JOURNAL OF THE AMERICAN CHEMICAL SOCIETY

Article

pubs.acs.org/JACS

A Study of Phenylalanine Side-Chain Dynamics in Surface-Adsorbed Peptides Using Solid-State Deuterium NMR and Rotamer Library Statistics

Kun Li,[§] Prashant S. Emani,[‡] Jason Ash,[‡] Michael Groves,[§] and Gary P. Drobny*[,‡]

[‡]Department of Chemistry, University of Washington, Box 351700, Seattle, Washington 98195, United States
[§]Department of Physics, University of Washington, Box 351560, Seattle, Washington 98195, United States

Supporting Information

ABSTRACT: Extracellular matrix proteins adsorbed onto mineral surfaces exist in a unique environment where the structure and dynamics of the protein can be altered profoundly. To further elucidate how the mineral surface impacts molecular properties, we perform a comparative study of the dynamics of nonpolar side chains within the mineral-recognition domain of the biomineralization protein salivary statherin adsorbed onto its native hydroxyapatite (HAP) mineral surface versus the dynamics displayed by the native protein in the hydrated solid state. Specifically, the dynamics of phenylalanine side chains (viz., F7 and F14) located in the surface-adsorbed 15-amino acid HAP-recognition fragment (SN15: DpSpSEEKFLRRIGRFG) are studied using deuterium magic angle spinning (^{2}H MAS) line shape and spin−lattice relaxation measurements. ^{2}H NMR MAS spectra and T_1 relaxation times obtained from the deuterated phenylalanine side chains in free and HAP-adsorbed SN15 are fitted to models where the side chains are assumed to exchange between rotameric states and where the exchange rates and a priori rotameric state populations are varied iteratively. In condensed proteins, phenylalanine side-chain dynamics are dominated by 180° flips of the phenyl ring, i.e., the "π flip". However, for both F7 and F14, the number of exchanging side-chain rotameric states increases in the HAP-bound complex relative to the unbound solid sample, indicating that increased dynamic freedom accompanies introduction of the protein into the biofilm state. The observed rotameric exchange dynamics in the HAP-bound complex are on the order of 5−6 × 10^6 s^{-1}, as determined from the deuterium MAS line shapes. The dynamics in the HAP-bound complex are also shown to have some solution-like behavioral characteristics, with some interesting deviations from rotameric library statistics.

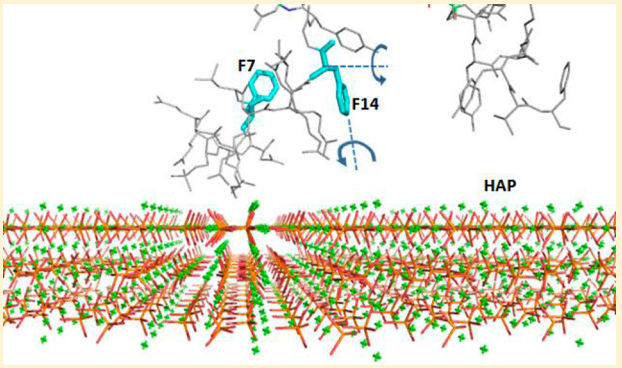

1. INTRODUCTION

There is growing interest in the structures of proteins at biomineral interfaces and how the secondary and tertiary motifs assumed by these surface-adsorbed molecules regulate the forms and properties of mineral-based hard tissues such as diatom frustules, mollusk shell nacre, bones, and teeth.[1] When adsorbed onto calcite or hydroxyapatite (HAP) surfaces or introduced into solutions of silicic acid, these proteins act as catalytic collection points or provide structural templates[2] which induce or in some cases inhibit formation of the solid biomineral phase. In addition a number of spectroscopic studies including NMR, SFG, and NEXAFS indicate that the side chains of these proteins provide the direct means by which interactions with these mineral phases are formed.[3−8]

It is also well-known that proteins in many biological contexts do not exist as static forms but undergo internal motions that modulate both their secondary and tertiary structures. In many cases these internal motions result in structural rearrangements that are necessary for function. Models of biomineralization proteins adsorbed onto mineral surfaces obtained recently by structural computations provide a picture of protein−surface recognition based on patterns of interactions between polar side chains of the protein and surface phosphate triads.[9] Structural computations guided by solid-state NMR structural data suggest that these interactions provide a basis for crystal face specificity if the surface recognition domain is well-structured.[3,4] These models also suggest that binding to different crystal faces is accompanied by changes in the conformations of protein side chains in close proximity to the mineral surface, so the structures of biomineralization proteins and the amino acid side chain within these proteins must retain a degree of mobility to adapt to different surface conditions. To better understand the nature of the interactions between protein side chains and biominerals and the role that motions of the protein main chain and side

Received: May 9, 2014
Published: July 23, 2014

   dx.doi.org/10.1021/ja504677d | J. Am. Chem. Soc. 2014, 136, 11402−11411

chains play in the formation of interactions with biomaterial surfaces, we explore the following: (1) the degree to which surface-adsorbed protein structures are modulated by motions; (2) how these motions differ from the movements of the same structural moieties in the native proteins; (3) the degree to which proximity to the surface and interactions with the surface are reflected in perturbations of molecular motions; (4) the degree to which the surface adsorption restricts or enhances motions of the protein structure.

Solid-state NMR is now widely used to study the dynamics of proteins in various physical states including hydrated amorphous powders,[10] microcrystals,[11] fibrils,[12] as well as membrane-associated proteins and peptides.[13,14] Quantifying dynamic rates and amplitudes is especially straightforward using deuterium solid-state NMR (^{2}H ssNMR).[15−17] To a very good approximation, the solid-state ^{2}H ssNMR spectrum is dominated by a single interaction: that of the electric quadrupole moment of the ^{2}H nucleus with surrounding electric field gradients. The magnitude of this interaction is quantified by the deuterium quadrupolar coupling constant (i.e., QCC= (e^2qQ/h), which is on the order of ∼160−200 kHz for deuterons in carbon−deuterium bonds[18] and about 180 kHz for phenylalanine ring carbon−deuterium bonds of interest in this work.[19] Given the magnitude of the anisotropy of the deuterium quadrupolar interaction, very fast motions (correlation times τ_c < 100 ns) can be probed by Zeeman spin−lattice (i.e., T_{1Z}) and quadrupolar (T_{1Q}) relaxation measurements, while motions with longer correlation times dynamically perturb ^{2}H NMR line shapes. In addition protein motions can be probed by solid-state deuterium NMR at individual amino acid side chains using site-specific deuteration.

Despite its usefulness as a probe of molecular dynamics, ^{2}H ssNMR has practical limitations. The large anisotropy of the quadrupolar interaction and the small size of the deuterium spin magnetic dipole moment result in low sensitivity which makes difficult the extension of ^{2}H ssNMR to large macromolecular systems with high deuterium dilution, such as selectively deuterated proteins adsorbed onto biomaterial surfaces. Deuterium magic angle spinning (^{2}H MAS) NMR has emerged in recent years as a viable alternative to static quadrupolar echo spectroscopy. Spinning a deuterated sample rapidly around a goniometer, whose axis is oriented at 54.74° (i.e., the magic angle) relative to the direction of the static external magnetic field, breaks the ^{2}H NMR solid-state line shape into side bands separated by intervals of the spinning frequency ν_R, where typically 1 kHz < ν_R < 20 kHz. Because the integrated intensity of the ^{2}H NMR spectrum is concentrated into a small number of side bands in a MAS experiment, sensitivity enhancements of 20−30 are easily achievable. This feature makes ^{2}H MAS NMR a potentially powerful approach for studying the dynamics of very small quantities of selectively deuterated biopolymers. At the same time, we note that parallel approaches such as deuteron QCPMG experiments have also been used in recent work by Vugmeyster, Vold, and co-workers to elucidate side-chain dynamics of residues in the hydrophobic core of a chicken villin headpiece subdomain.[20−22]

We have shown that ^{2}H MAS NMR yields high signal-to-noise spectra for so-called LK peptides adsorbed at monolayer coverage on polystyrene and carboxylated polystyrene surfaces. In these model systems the MAS line shape is indicative of the orientation of LK peptides adsorbed onto functionalized polymer surfaces.[7,23,24] In this manuscript we extend ^{2}H MAS NMR to the study of amino acid side-chain dynamics in a biomineralization protein adsorbed onto its native mineral surface. Salivary statherin is a 43-amino acid proline- and tyrosine-rich phosphopeptide found in the submandibullar saliva.[25−29] Statherin has the dual function of inhibiting both nucleation and crystal growth of hydroxyapatite [$Ca_{10}(PO_4)_6(OH)_2$, (HAP)] in the oral environment.[30] Statherin also acts as a boundary lubricant and has been found to have bacterial binding domains for *Porphyromonas gingivalis*[31] and *Actinomyces viscosus*.[32] The N-terminal 15 amino acids (i.e., SN15: DpSpSEEKFLRRIGRFG, pS = phosphoserine) constitute the HAP recognition domain of statherin.[33−35] If SN15 is deleted from statherin, the HAP binding affinity is markedly decreased. The HAP binding affinity of SN15 itself is almost as large as that of statherin.[36]

The structures of both SN15 and statherin adsorbed onto HAP crystals have been studied by solid-state NMR dipolar recoupling techniques.[36,37] The segment of statherin containing SN15 when bound to HAP is helically structured, although the secondary structure is distorted from a classical α-helix. The distorted helical structure appears to optimize exposure of several polar amino acid side chains to the HAP surface including E4, K6, R9, and R10.[9,38] Molecular modeling with the program RosettaSurface constrained by ssNMR dipolar recoupling data shows that the majority of the nonpolar side chains in statherin's HAP recognition domain: F7, L8, I11, F14, are more remote from the HAP surface.[3] In SN15, however, distortion of the helical structure near the C-terminus allows the phenyl ring of F14 to orient close enough to the HAP surface to produce a ^{13}C{^{31}P} REDOR response.[36] Analysis of the REDOR data shows that the phenyl ring of F14 is around 4−5 Å from HAP surface phosphate groups. No REDOR signal is observed for the phenyl ring of F7 in SN15 so the ^{13}C spins in this phenyl ring are >7 Å from the nearest HAP surface phosphate groups.

It is the differing surface exposure of the two phenylalanine side chains in SN15 (compared to statherin where both phenylalanine rings are distant from the HAP surface) that presents us with the opportunity to study the effects of the mineral surface environment and surface proximity on side-chain dynamics: specifically, we can understand the behavior of differently oriented hydrophobic side chains in the presence of a hydrophilic surface. The interest in phenylalanine rings is further heightened by the observation that phenylalanine was found to have highest affinity to HAP among four amino acids with hydrophobic side chains.[39] In this manuscript, we obtain ^{2}H MAS line shapes for microcrystalline SN15 molecules selectively deuterated on the phenyl rings of F7 and F14 unbound, as well as bound to HAP crystal surfaces. We analyze these dynamically averaged line shapes and T_1 data by assuming side-chain motions consist of exchange between discrete rotameric states of the phenylalanine side chains. We show the degree to which surface adsorption perturbs side-chain mobility in proteins and the more subtle effects exerted in HAP-adsorbed proteins when phenylalanine side chains are exposed to the HAP surface to differing degrees. This study gives a high resolution view of how the mineral surface impacts protein side-chain motions and how these motions differ very strikingly from motions of phenylalanine side chains in solid, hydrated proteins. Finally, another reason for choosing SN15 over statherin is the availability of data from a recent NEXAFS study of the same side chains in SN15 adsorbed onto a planar HAP surface,[8] and we compare and contrast our results to these. We also compare the choice of rotameric states obtained

herein to the computational models obtained from Rosetta-Surface.NMR[3] and to a previous solution-state study[40] of phenylalanine conformers. We find similarities between the statherin computational models and the solution conformers, with a noteworthy deviation in the case of our models for F14 in SN15. Close proximity to the surface, as for F14 in SN15, simultaneously increases conformational freedom relative to the unbound solid-state while not entirely reflecting solution-like behavior.

2. MATERIALS AND METHODS

Peptide Synthesis. *Materials.* Protected amino acids and Fmoc-Gly-Wang resin were purchased from Calbiochem Novabiochem Corp. (San Diego, CA). [Ring-$^2H_5$] L-phenylalanine was purchased from Cambridge Isotope Laboratories, Inc. (Andover, MA). HAP (55 m^2/g) was synthesized by Allison Campbell at Pacific Northwest National Lab as published previously.[35]

Peptide Synthesis and Characterization. Both [ring-^{2}H5]-labeled phenylalanine SN15 samples were prepared as follows. [Ring-^{2}H5] L-phenylalanine was FMOC protected using standard procedures.[41] From a preloaded Fmoc-Gly-Wang resin (substitution 0.60 mmol/g), the SN15 peptide was synthesized on a Rainin PS3 automated solid-phase peptide synthesizer (Protein Technologies, Inc.), where the solvent was *N*,*N*-dimethylformamide (DMF), the activator was 0.4 M *N*-methylmorpholine in DMF and the deprotector was 20% (v/v) piperidine in DMF. The acidic portion of SN15 (D1 to K6) was double coupled, while the rest of the peptide was built through single couplings. The peptide was cleaved from the resin using a 9.5 TFA:0.25 H_2O:0.25 TIS (triisopropylsilane) solution following method 3-18 described in the Novabiochem 2002/3 catalog.52. Using a Waters HPLC C-18 reverse phase column, the peptide was purified with an acetonitrile/water solvent system with 0.1% TFA, eluting at 35.4% acetonitrile, lyophilized, and then analyzed by MALDI mass spectrometry to establish composition and purity.

Peptide Adsorption to HAP. SN15 was physisorbed to HAP by mixing a solution composed of 0.05 mM of peptide in a phosphate buffer with about 100 mg of HAP (55 m2/g). The pH of the mixture was adjusted to 7.4 with NaOH and HCl. The phosphate buffer was 100 mM NaCl, 40 mM KCl, 1.4 mM KH_2PO_4, and 4.3 mM Na_2HPO_4. After 4 h of mixing, the unbound peptide was separated from the peptide−HAP complex though centrifugation. The peptide−HAP sample was washed several times with buffer, lyophilized, and then packed in the rotor for solid-state NMR studies.

NMR Experiments. Solid-state NMR experiments were performed on a home-built solid-state NMR spectrometer equipped with a 9.4 T magnet (61.5 MHz. deuterium Larmor frequency) using a Varian T3MAS probe and 4 mm sample rotors. For MAS experiments, samples were spun at 8 kHz (regulated to within ±5 Hz by a spin-rate controller). A single $\pi/2$ pulse (2.5 μs in length) was applied followed by acquisition of the rotary echo train. After left-shifting to the peak of the first echo, FIDs were Fourier transformed and phase corrected. All line shapes have a Lorentzian broadening of 1 kHz. All measurements were made at three different temperatures, −30 °C, 20 °C, and 60 °C. For the T_1 experiments, we used a simple inversion−recovery pulse sequence with a π pulse length of 5.5 μs. The π pulse was followed by a delay which is used to recover the magnetization. Then the single $\pi/2$ pulse was applied followed by acquisition. For the free peptide, the delay time was set to nine different time points, and the relaxation time between acquisitions was carefully chosen to be 4 s; for the bound peptide, the delay time was also set to nine different time points, but the relaxation time between acquisitions was set to 0.4 s.

Deuterium MAS Line Shape and T_1 Simulations and Dynamic Models. *Simulation Algorithm.* ^{2}H NMR MAS spectra and inversion−recovery experiments were simulated with an in-house program, KLDMAS. The theory of KLDMAS, based on an approach developed by Duer and Levitt,[42] has been described in detail in previous publications,[7,23] and we provide a brief summary in the Supporting Information. The process of MAS line-shape simulation was automated following the general strategy of Nielsen and co-workers[43] and involves comparison of the experimental spinning side bands' intensities to simulated intensities. To optimize fits to experimental data, a set of parameters was varied iteratively, and the acceptance of a new parameter set is determined by annealing methods.[44] In addition to line-shape simulations, KLDMAS is also used to simulate inversion recovery MAS experiments.

Models for Phenylalanine Side-Chain Dynamics in Unbound and HAP-Bound SN15. The motion of the phenylalanine ring could potentially involve the multiaxial dynamics resulting from a combination of backbone and side-chain flexibility. However, previous work in the group has shown that, in both unbound and HAP-bound SN15 samples, lyophilization results in a fairly rigid peptide backbone.[35] In that study, it was found that while ^{13}C CSA and ^{13}C $T_{1\rho}$ measurements on the backbone carbonyl groups of the hydrated sample did indeed show motions in the C-terminal end of the SN15, corresponding measurements on lyophilized samples indicated that the molecule did not exhibit any significant motions on a time scale less than 10^{-3} s.[35] Also, as shown below, the T_1 relaxation times reported in this manuscript for the bound molecule did not show the existence of two or more components, implying that there is no evidence for multiple populations of either backbone carbonyl bonds or the fast-flipping ring bonds in the HAP-bound molecule. The remaining possibility that differing hydration states for the surface-bound molecule lead to multiple rotameric distributions, such as a bound (rigid) and an unbound (mobile) population in the same sample, is unlikely given REDOR measurements on F7 and F14: Gibson et al.[36] were able to fit the data for a single average distance. Finally, we do advise that the models herein are subject to the same limitations as any well-justified model-based approach.

Thus, in our current work we focus only on models involving side-chain conformational changes. As shown in Figure 1a, the conformational state of the phenylalanine side chain is quantified by two-bond dihedral angles: χ_1 and χ_2. χ_1 is defined as the angle between the N−C_α−C_β and C_α−C_β−C_γ planes and thus quantifies the rotational state of the C_α−C_β bond. The rotational state of the C_β−C_γ bond is described by χ_2, which is defined as the angle between the C_α−C_β−C_γ and the C_β−C_γ−$C_{\delta 1}$ planes. Motions of the phenylalanine side chain are quantified by ascribing time dependence to one or both of these angles.

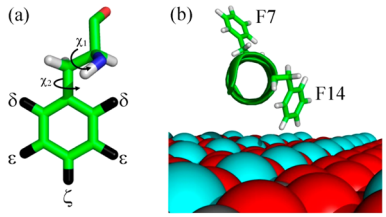

Figure 1. (a) Model of phenylalanine. The deuteration sites are denoted in black, along with the two rotational axes. (b) A model of SN15, indicating the close proximity of the phenylalanine residue at position 14 to the HAP surface.

An extensive literature search shows that in solid monomeric form and in solid peptides and proteins, the dynamics of the phenylalanine side chain is dominated by exchange of the phenylalanine ring between two discrete states of χ_2 related by 180°, the so-called "π flip"[45−47] which changes drastically the orientation of the δ and ε C−D bonds but leaves invariant the ζ C−D bond orientation. Accordingly, in this manuscript we use the "π flip" dynamic model of phenylalanine side-chain motion to simulate the motions of the aromatic rings of F7 and F14 in the microcrystalline, unbound SN15. The NMR observables are assumed to be powder-averaged.

To fit fully and partially relaxed deuterium line shapes for phenylalanine side chains in unbound SN15, the parameter set consists of the deuteron QCC and the "π flip" exchange rate. In the π flip model the two values of χ_2 are assumed to have equal a priori populations. No other motions need be invoked to simulate the ^{2}H

dx.doi.org/10.1021/ja504677d | J. Am. Chem. Soc. 2014, 136, 11402−11411

line shapes and relaxations times for deuterated F7 and F14 in unbound SN15. See Supporting Information.

However, the ^{2}H MAS line shapes and spin−lattice relaxation times observed for the F7 and F14 side chains in HAP-adsorbed SN15 indicate that the motions of these moieties differ markedly from the motions of the same side chains in unbound SN15. To simulate the line shapes for deuterated F7 and F14 in HAP-bound SN15, a model was designed that includes rotational motions around both the C_α−C_β bond (where the χ_1 dihedral angle varies) and the C_β−C_γ bond (where the χ_2 dihedral angle varies) in addition to the π flip of the C_β−C_γ bond. We assume that the rotational motions of the C_α−C_β and C_β−C_γ bond consist of rotameric exchanges. The parameter set for our model of phenylalanine side-chain dynamics in HAP-bound SN15 includes the deuteron QCC, the π flipping rate, rotameric-state populations, side-chain bond dihedral angles that characterize each exchanging rotamer, and the rates of exchange between side-chain rotamers. Initial values for rotameric-state populations and dihedral angles are obtained from the backbone-dependent rotamer library of Shapovalov and Dunbrack.[48]

Dynamic models based on rotameric exchange have been used widely to simulate solid-state ^{2}H NMR line shape and relaxation data acquired from amino acid side chains in proteins, notably deuterons within the side chains of leucines and valines. In some cases exchange is restricted to side-chain rotamers that are observed to be dominant in crystal structures as was done by Torchia and co-workers[12] and more recently by Vugmeyster, Vold, and co-workers.[20,22,49] To generalize this approach, we have utilized protein side-chain rotamer libraries which show that for bonds between sp^3-hybridized carbons, dihedral angles occur in tight clusters typically around angles of 60°, 180°, and 300° (i.e., gauche+, trans, gauche−). Depending upon the amino acid side chain in question, the exact location and shape of maxima in the side-chain bond dihedral distributions vary by at most 20° with standard deviations usually less than 10° in high-resolution structures.[48] In the case of phenylalanine, for α-helical secondary structures (i.e., $\phi = -50°$, $\psi = -40°$) the C_α−C_β bond dihedral angles are clustered near ideal rotameric values, i.e. $\chi_1 = 179.8 \pm 9.1°$ with a probability of 0.721, $\chi_1 = 286 \pm 10.8°$ with a probability of 0.254, and $\chi_1 = 75.4 \pm 8.1°$ with a probability of 0.025. In contrast, bonds between sp^3- and sp^2-hybridized carbons in protein side chains exhibit broad and often asymmetric probability density distributions. Accordingly, the rotamer library of Shapovalov and Dunbrack shows that the dihedral angle χ_2 for the C_β−C_γ bond in phenylalanine is broadly distributed among nonrotameric values within the interval $-30° < \chi_2 < 150°$.

To simulate the ^{2}H MAS line shapes for the bound peptide, we attempted fits to the data with models that included the three primary conformers, i.e., $\chi_1 = 179.8°$ (trans), $\chi_1 = 286°$ (gauche−) and $\chi_1 = 75.4°$ (gauche+). However, for both F7 and F14, when setting initially all three conformer populations to 1/3, the fitting procedure eventually drove the population of one of the three conformers to zero. Thus, we find that two conformers are sufficient for the purposes of fitting the data in this manuscript, without any a priori bias toward any of the rotamers.

The χ_1 angle for each conformer was explored as follows: we set up boundaries of ±30° around the rotamer library values mentioned above; then we allowed the search algorithm to take steps of size $\sigma \times rand$, where σ is the standard deviation of that conformer (given above for each of the three conformers), and *rand* is a random number in the interval [−1, 1]. If the new angle provided a better match to the line shape, this angle was accepted and the process was iterated with this as the new starting point. Over time, the step size was decreased by a simulated annealing parameter. If the search algorithm was unable to improve the fit significantly after several steps, and remained close to one of the ±30° boundary walls, we expanded the walls to a larger value and repeated the procedure. Because the χ_2 angle in phenylalanine is not confined to specific rotameric values, this angle was freely varied. With regard to the δ/ε deuterons, the resulting model consists of a four-site exchange, which combines a conjoint rotameric exchange motion of the C_α−C_β and C_β−C_γ bonds between two sites together with a π flip of the C_β−C_γ bond. The impact of these exchanges between rotameric states on the deuterium line shape is significant. Although the orientation of the C−D bond containing the ζ deuteron is invariant to rotations around the C_β−C_γ bond axis, including the π flip motion, its orientation varies when the C_α−C_β bond exchanges between the rotameric states.

The quadrupolar coupling constant (QCC) for the deuterons was treated as a free parameter, after starting at literature-reported values of around 180 kHz (see for example Gall et al.[19]).

3. RESULTS

Model Parameters for Phenylalanine Side-Chain Dynamics in Unbound SN15. The line shapes and relaxation times for F7 and F14, as well as the full simulation parameters for multiple sample temperatures, are presented in the Supporting Information. In Table 1, we provide the simulation parameters for unbound SN15 at T = 293 K.

Table 1. Simulation Parameters for ^{2}H Line Shape of Deuterons of F7 and F14 in Unbound SN15

simulation parameter	F7 static parameters	F7 flipping parameters	F14 static parameters	F14 flipping parameters
QCC (kHz)	175.0	175.0	175.0	175.0
asymmetry parameter	0.06	0.06	0.06	0.06
flipping rate (293 K)	0	1.4×10^7	0	3.0×10^7
intensity percentage (293 K)	75%	25%	79%	21%

We note that the models chosen here are the minimally sufficient models to explain the data, i.e., we have demonstrated that the measured line shapes and relaxation times can both be entirely explained by previously proposed models of a population of π-flipping and a population of nonflipping phenylalanine rings.[11,19,45,50] This model does not preclude the existence of very slow exchange motions between the two types of rings, static and flipping, nor between different side-chain rotamers. However, such exchange rates are likely to be much slower than the rates accessible by the MAS line shapes, given our ability to model our data without invoking additional motions. We discuss our choice of unbound models further in the Supporting Information.

Line Shapes and Simulations for Phenylalanine Side-Chain Dynamics in HAP-Bound SN15. ^{2}H MAS line-shape data acquired for F7 and F14 side-chain deuterons in HAP-adsorbed SN15 at T = 293 K are shown in Figure 2, parts a and b, respectively, with the corresponding best-fit simulations in (c) and (d). (The line shapes for SN15 bound to HAP at temperatures of 243 and 333 K are shown in the Supporting Information Figure S3. However, the variation in the line shapes as a function of temperature was not significant, and thus the fit parameters as a function of temperature are not shown.) The comparison with Supporting Information Figure S1 indicates that the side chain in the surface-adsorbed protein behaves differently from that in the unbound protein. In particular, the line shapes in Figure 2 display clearly the absence of the static component as in the unbound line shapes, indicating the existence of additional motions of the side chain that have averaged and/or attenuated the δ/ε and ζ deuteron signal.

In each line-shape simulation, adjustable parameters include the side-chain conformation populations, the exchange rate constant, and χ_1 and χ_2 torsion angles. The side-chain

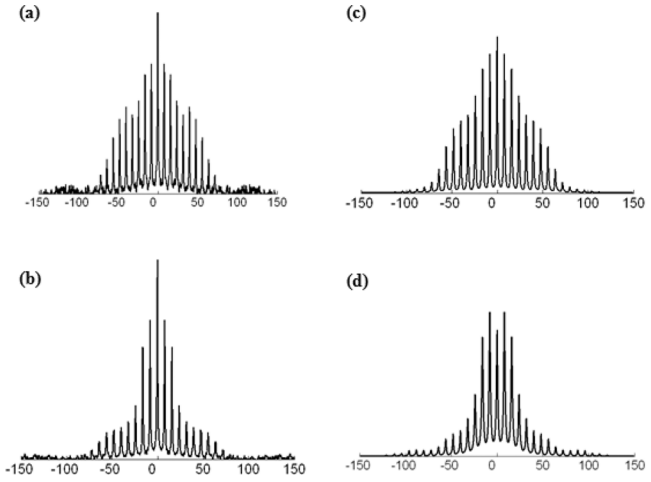

Figure 2. Experimental spectra of F7/F14 in SN15 peptides bound to HAP at room temperature vs simulations: (a) MAS spectrum of bound F7; (b) MAS spectrum of bound F14; (c) MAS simulation of bound F7; (d) MAS simulation of bound F14. The intense peak in the center of the experimental spectra arises in part from surface-adsorbed HDO.

conformation populations are related in the rate matrix by $R_{ij} = k(P_i/P_j)^{1/2}$ where P_i and P_j are the populations of rotamers i and j, respectively, and k is the exchange rate constant. Initial χ_1 and χ_2 torsion angles are derived from the rotamer libraries and are subject to change within preset boundaries iteratively during each simulation.

In addition to geometric parameters for the rotameric exchange motions of the $C_\alpha-C_\beta$ and $C_\beta-C_\gamma$ bonds, the scale of the π flip motion rate is found in a manner similar to the unbound case. Table 2 shows T_1 measurements acquired for

Table 2. Spin−Lattice Relaxation Times T_1 for the δ/ε Deuterons as a Function of Temperature

residue	average T_1 (ms) at T = 243 K	average T_1 (ms) at T = 293 K	average T_1 (ms) at T = 333 K
F7	18.6 ± 4.2	21.6 ± 3.5	40.0 ± 14.3
F14	32.5 ± 5.8	46.4 ± 6.8	50.5 ± 8.3

the δ/ε ring deuterons of F7 and F14 as a function of temperature. Unlike the unbound case, the relaxation times increase with temperature, indicating that the flipping rates have shifted to a motion range greater than the ^{2}H Larmor frequency, and consequently dominate the relaxation. We justify this assumption of a predominant motion on the T_1 time scale on the grounds that while the π flip exchanges the ring between essentially equivalent physical orientations, rotameric exchange moves the entire bulk of the side chain between discrete and distinguishable sites. Fitting the T = 293 K data for the F7 and F14 δ/ε deuterons to a two-site jump model results in a π flip of the F7 and F14 rings in the rate range 10^9 to 10^{10} s^{-1}. The π flip rates determined from the T_1 measurements were not adjusted further during the line-shape simulations. Final parameter sets corresponding to the best fit are in Tables 3 and 4.

The data for both F7 and F14 evince a correlation between the best-fit χ_1 and χ_2 angles, with the exchange between conformers necessitating a simultaneous modification of both angles. Possible sources of such a correlation include a change in the steric or electrostatic interaction of the ring with other parts of the protein and/or the surface upon transitioning from

Table 3. Exchange Rates, Quadrupolar Coupling Constants and Asymmetry Parameters Used To Simulate the ^{2}H MAS Line Shapes of the Ring Deuterons of F7and F14 in HAP-Bound SN15

parameters for HAP-bound phenylalanines	F7 ζ deuteron	F7 δ/ε deuterons	F14 ζ deuteron	F14 δ/ε deuterons
QCC (kHz)	183.0	183.0	182.3	182.3
asymmetry parameter	0.06	0.06	0.06	0.06
rotamer exchange rate constant (s^{-1})	5×10^6	5×10^6	6×10^6	6×10^6
ring flipping rate constant (s^{-1})	none	5.6×10^9	none	2.6×10^9

Table 4. Parameters for Best-Fit HAP-Bound Conformers for F7 and F14 Residues

F7 conformers	χ_1 (deg)	χ_2 (deg)	population (%)
conformer1	186.2	88.6	76.1
conformer2	274.7	54.8	23.9
F14 conformers	χ_1 (deg)	χ_2 (deg)	population (%)
conformer1	93.1	208.8	40.9
conformer2	273.6	56.8	59.1

one conformer to the next. It is even possible that the interaction with residual water in the local environment changes between the two conformers.

While the results in Table 4 are presented in terms of the χ_1 and χ_2 angles of the side-chain conformers, it is to be borne in mind that fitting line shapes and relaxation data can only yield *differences* in angular values and not the absolute values. The absolute values were obtained by varying the angles near the rotamer library values, but there can still be a small degree of degeneracy in the models as long as the best-fit differences in the torsion angles are maintained. Furthermore, in Figure 3 we provide a plot of the χ^2 surface for F7 (Figure 3a) and F14 (Figure 3b) in the vicinity of the best-fit χ_1 and χ_2 angles of conformer 2, assuming the best-fit value of the angles for conformer 1, to provide an idea of the degree of discrimination between alternative models in the vicinity of the minima provided in Table 4. It can be seen from that the χ^2 surface for F7 is more complicated than that for F14. However, the χ^2 value of the final choice of angles was ∼1.5 times less (F7) and ∼2 times (F14) less than that of the next lowest minimum.

4. DISCUSSION

We have shown that the motions of phenylalanine side chains in the HAP-recognition domain of statherin (i.e., SN15) differ significantly between the unbound and the surface-bound states, indicating that the local free energy surface of the side chain is modified from one sample condition to another. The side-chain motions in the unbound state of SN15 are well fitted by a model used in a number of previous studies of phenylalanine ring motion in solid proteins, where a fraction of the phenyl rings execute 180° flips, while the remaining rings are prevented from undergoing motions faster than time scales on the order of a millisecond (the longest time scale of sensitivity for the deuterium line shape). Surprisingly, the HAP-bound SN15 peptide shows a flexibility greater than that of the unbound SN15 with the entire side chain exchanging between different conformers by rotations around the $C_\alpha-C_\beta$ and $C_\beta-C_\gamma$ bonds together with all the phenyl rings undergoing ring 180° flips. We explore below some aspects of the bound models and construct a more complete physical picture of the

dx.doi.org/10.1021/ja504677d | J. Am. Chem. Soc. 2014, 136, 11402−11411

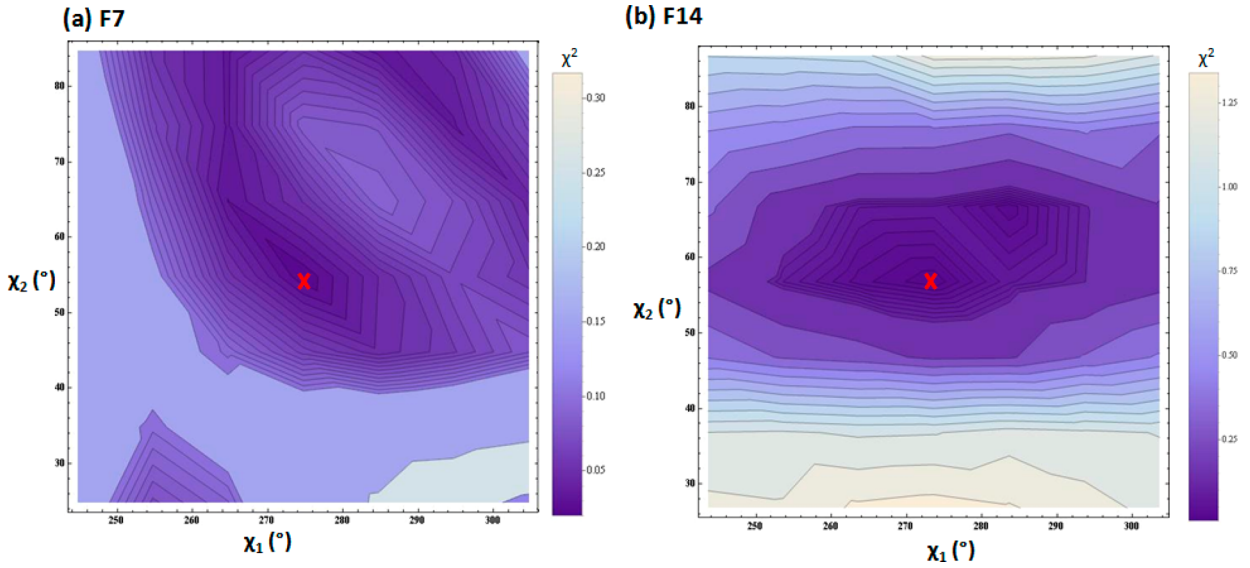

Figure 3. χ^2 plot as a function of the χ_1 and χ_2 angles of "conformer 2" from Table 4 assuming the best-fit values for "conformer 1": (a) F7 and (b) F14. The best-fit values displayed in Table 4 are marked by a red cross. The range explored for each angle is ±30° from the best-fit values. The spacing of the contours is not fixed, with the contours of the lower values of χ^2 being more closely spaced than those of the higher values for the sake of clarity.

dynamical state of the phenylalanine residues in the HAP-bound peptide using previously published results in conjunction with our own. We will also discuss how there are similarities between the bound-state dynamics and solution-state dynamics of phenylalanine side chains.

HAP-Bound Dynamics. As discussed in the Supporting Information, the existence of a population of nonflipping phenyl rings in some solid proteins has been attributed in the literature to the packing of the molecules in conjunction with coordinated water. However, the HAP-bound models no longer require the invocation of such a population, indicating in the environment of the HAP surface that all phenyl rings undergo π flips. Moreover, as seen from the simulation parameters, the rate of this flipping increases significantly in going from the unbound to the HAP-bound state.

Our study also finds that rotameric exchange motions (within the range of rates explored here) of the $C_\alpha-C_\beta$ and $C_\beta-C_\gamma$ bonds are properties only of the HAP-bound SN15 peptide. The process of iteratively fitting the ^{2}H NMR line shapes and relaxation times of HAP-bound SN15 to a rotameric model is initialized by assigning rotameric populations found in crystal-based rotameric libraries and then subsequently modifying the populations using an annealing algorithm. In support of using crystal-based rotamer libraries in a surface-bound environment, we note that RosettaSurface.NMR utilizes such rotamer libraries (see Supporting Information in Masica et al.[51]) with subsequent side-chain repacking to simulate effects imposed by the surface. This same strategy was used in a more recent study by Masica, Gray, and co-workers[52] where RosettaSurface was used to design de novo six peptides intended to bind to and alter the crystallization of calcite. All six peptides dramatically affected calcite crystal growth (as observed by scanning electron microscopy), and the effects were dependent on the state of the {001} growth plane as targeted by the algorithm. Moreover, rotamer libraries are compendia of side chains in a wide variety of intrapeptide environments which, taken together with an allowance for deviation (at least ±30° in the case of χ_1 and an even greater range for χ_2), justifies the use of crystal-based rotameric libraries in our analysis.

Interestingly, F7 exhibits a change in dynamics in the bound state relative to the solid state, even though it was found to be greater than 7 Å away from the HAP surface (and thus lacking a $^{13}C-^{31}P$ REDOR signal).[36] Clearly, this implies that some change in the free energy landscape occurs even for F7: this is a result either of a direct interaction of the phenyl ring with the surface, or an indirect one, where the conformation and orientation of the molecule as a whole is modified sufficiently to change the immediate environment of F7, or some combination thereof. As remarked with regard to the phenyl ring flipping, the surface binding process may interrupt networks of intermolecular and water molecule coordination, resulting in modified dynamics even for residues distant from the surface.

The models are also assumed to be the same across all peptides in the sample. Given that the HAP surfaces in the experiment were potentially heterogeneous, this assumption could be called into question, especially for the HAP-proximal F14. However, F14 REDOR data from Gibson et al.[36] is well fit by a distance that varies only by about 0.5 Å, and while this may still represent an average over rapidly exchanging positions of the ring, it does not support a broad static distribution of ring–surface distances. Any dynamic heterogeneity would have to accord with this constraint on average distance. In addition, the work of Masica et al. shows a binding preference for statherin for three HAP crystal faces out of five tested, leading to a further reduction in possible heterogeneity. While this still allows for a certain degree of diversity in motion, we choose to present a single model of motion in this paper as the simplest possible explanation of the data.

It is helpful to examine the models used in this study in light of other methodologies used to study HAP-bound SN15. Here we compare the results of our ^{2}H NMR study to computational modeling[3] and NEXAFS[8] studies of the orientations of these same side chains for HAP-bound statherin and SN15. The orientations of phenylalanine side chains in the HAP

dx.doi.org/10.1021/ja504677d | J. Am. Chem. Soc. 2014, 136, 11402–11411

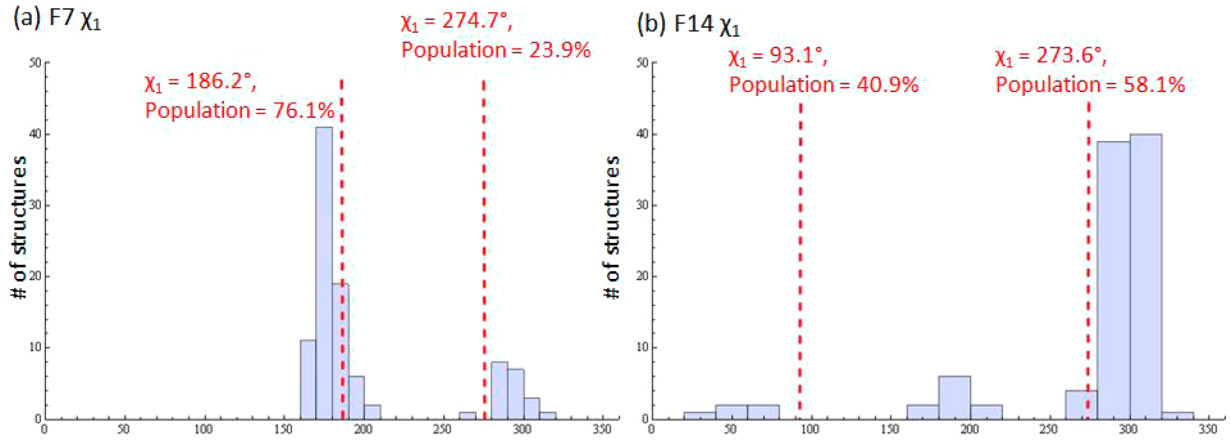

Figure 4. χ_1 distributions for the RosettaSurface.NMR structures overlaid with the values for χ_1 and the corresponding populations found for the best-fit conformers in the rotamer exchange model discussed in the current manuscript: (a) F7 distributions; (b) F14 distributions.

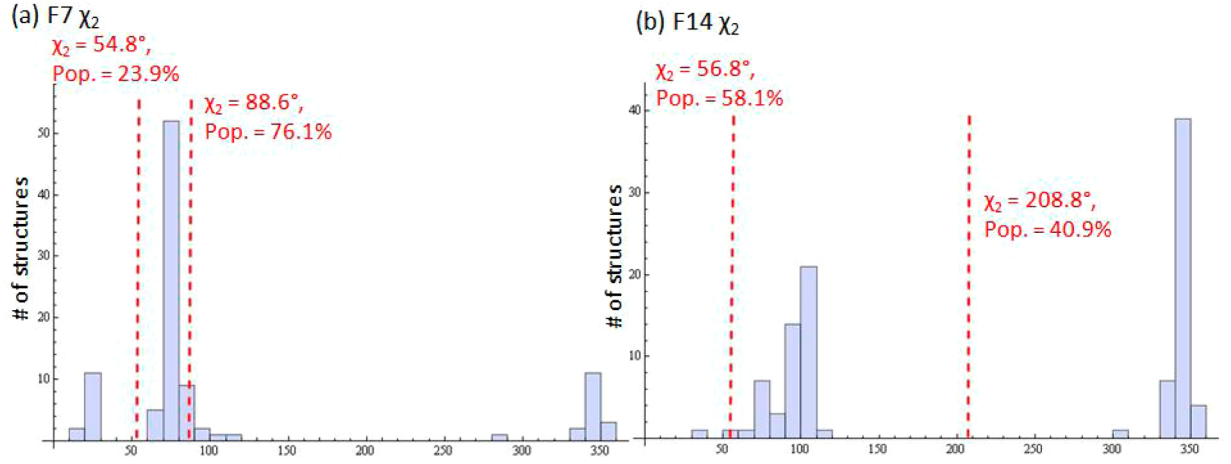

Figure 5. χ_2 distributions for the RosettaSurface.NMR structures overlaid with the values for χ_2 and the corresponding populations found for the best-fit conformers in the rotamer exchange model discussed in the current manuscript: (a) F7 distributions; (b) F14 distributions.

recognition domain of statherin have been calculated by Masica et al.[3] using a RosettaSurface algorithm (RosettaSurface.NMR) steered by ssNMR-derived structural constraints, and also determined experimentally by Weidner and co-workers using NEXAFS.[8]

Comparisons to Previous Studies. In the following subsections, we try to provide consistent interpretations for our results in light of those of three previous studies of phenylalanine conformations and dynamics: (a) the RosettaSurface.NMR results of Masica et al.[3] for the full statherin molecule; (b) the results of a NEXAFS study by Weidner et al.[8] on SN15; (c) the solution NMR study of Bremi et al.[40] on the decapeptide antamanide. The conclusions can be summarized as follows: (i) the dynamics and conformation of F7 are consistent with other surface-bound studies, with a great deal of similarity to the solution studies, implying that for a phenylalanine oriented away from the surface, the behavior is both rotameric and similar to that in the solution state; (ii) the dynamics and conformation of the more proximal F14 residue differ somewhat between our results for SN15 and those of the computational studies of full statherin and the solution NMR analysis, with our results showing a greater degree of nonrotameric behavior; however, the intermediate strength binding of F14 to HAP (see Gibson et al. for discussion[36]) still seems to allow some similarities to solution conformers.

Comparison to RosettaSurface.NMR Study. To compare our results to those of Masica et al, we obtained the 100 lowest energy structures of HAP-bound statherin from the authors of the RosettaSurface.NMR study. Histograms of the χ_1 angles for F7 and F14 residues of the 100 RosettaSurface.NMR structures are shown in Figure 4, parts a and b, respectively. In the case of F7 the primary cluster of χ_1 angles occurs in the range of 160° to 210°, with a smaller cluster occurring in the range of 260° to 320° (Figure 4a). Upon overlaying the best-fit χ_1 angles from our analysis, we notice that the values we have obtained in our ^{2}H NMR study fall within the values obtained from the analysis of Masica et al. There is also a correlation between the relative probabilities of finding the F7 χ_1 angle within each of the clusters, quantified by the number of structures in each cluster, and the a priori populations observed for the two exchanging conformers. For the F14 residue (Figure 4b), there are three clusters of χ_1 angles. While the highest population conformer that we obtained (with χ_1 = 273.6°) does indeed fall close to the cluster peak, the second conformer falls somewhat outside of the range of observed structural possibilities.

The comparisons of results for the χ_2 angle (Figure 5) follow a similar pattern. For F7 (Figure 5a), the χ_2 angles of the two

dx.doi.org/10.1021/ja504677d | J. Am. Chem. Soc. 2014, 136, 11402−11411

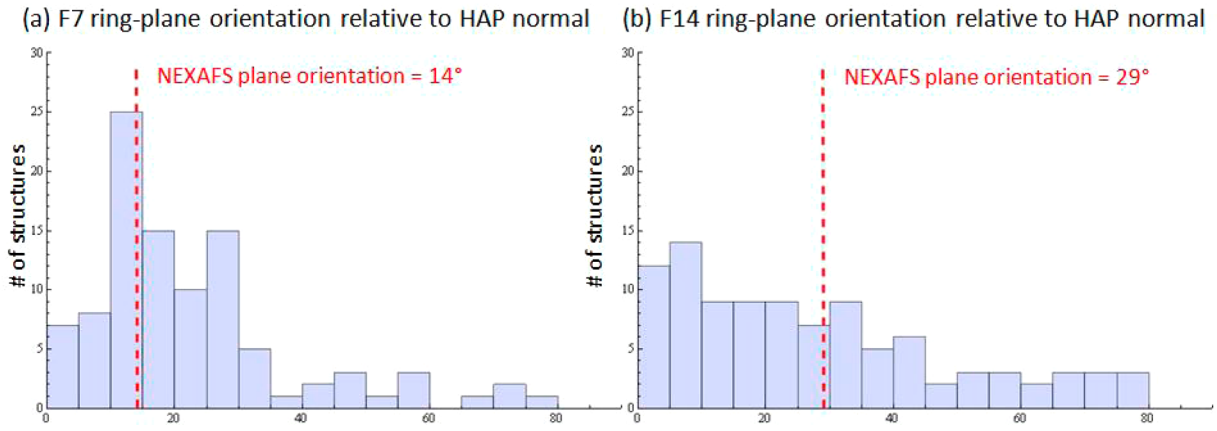

Figure 6. Phenyl ring-plane distributions for the RosettaSurface.NMR structures overlaid with the values for the plane orientations obtained from the NEXAFS study: (a) F7 distributions; (b) F14 distributions.

conformers fall near the primary cluster of the RosettaSurface.NMR structures, but for F14 (Figure 5b) the conformer with the lower population cannot be associated with any of the RosettaSurface.NMR clusters. The primary reason for the mismatch in the case of F14 is the difference in the proximities of F14 to the HAP surface in the SN15 fragment and in the full statherin molecule. On the basis of $^{13}C\{^{31}P\}$ REDOR data obtained for SN15 with ^{13}C-labeled phenylalanine incorporated at F7 and F14, Gibson et al.[36] found that the phenyl ring of F14 is on the order of 4.5 Å away from the phosphorus atoms on the HAP. In a similar REDOR study of the entire statherin protein adsorbed to HAP, Masica et al.[3] quote a value greater than 7 Å for the same distance. Gibson et al. state that there was an observed fraying of the α-helical secondary structure from residues 11−15 in the SN15 fragment which allows for the closer approach of F14 to the surface; while Masica et al. also observe a reduction in the helicity of the molecule in the vicinity of F14, the absence of a termination at residue 15 means that the secondary structure of the full statherin molecule prevents a similar close contact between F14 and HAP. Thus, in statherin bound to HAP, both F7 and F14 are distant from the surface, explaining why the positions of the observed clustering of the χ_1 and χ_2 angles in the RosettaSurface.NMR structures are very similar in value for both F7 and F14 (even if the relative populations are different).

Comparison to the NEXAFS Study. Given that the calculations in the current manuscript were carried out on data that are powder-averaged, as well as the lack of dependence of the dynamics simulation on the orientation of the HAP surface, we did not build a global picture of the orientation of the rings relative to the HAP normal. This means that a direct comparison to the NEXAFS results of Weidner et al.[8] is not possible. However, we can compare the orientations of the 100 RosettaSurface.NMR structures to the NEXAFS-experimental values and subsequently use the partial correspondence observed between our results and those based on the 100 structures for the χ_1 angles to tie together all three analyses into one coherent picture. Essentially, we use the backbone suggested by the RosettaSurface.NMR structures for the SN15 domain of statherin to compare our results to those of Weidner et al.

Figure 6 shows the results of the NEXAFS experiment overlaid on histograms for the orientations of the phenylalanine ring-planes relative to the HAP-surface normal. Weidner et al. define the angle ρ as the angle between the normal to the ring plane and the HAP surface normal and find values of $\rho = 76°$ for F7 and $\rho = 61°$ for F14. Here we define the orientation of the plane of the ring itself as $(90° - \rho)$. As can be seen in Figure 6a, the NEXAFS result for the F7 ring-plane orientation very clearly matches the distribution of ring-plane orientations from the 100 lowest-energy structures, with the NEXAFS value lying on top of the highest population bin. The average obtained over all 100 structures was 22.4° and so deviates from the experimental value by over 8°. The results for F14 (Figure 6b) are a little more ambiguous. The distribution of orientations across the 100 structures is broad, with a slight excess for values close between 0° and 10°. The average over all 100 structures is 27.7°. Interestingly, the average in the case of F14 is closer to the NEXAFS experimental value rather than the magnitude of the highest population bin. We see two possible explanations for the observed difference in the F7 and F14 data: one, further sampling of structures may yield a preference for orientations in F14 near 29°, indicating that both rings sample favored ring-plane orientations; or, second, there is a genuine difference in the behaviors of the two rings, with F7 being more constrained to be in a particular orientation, and F14 sampling a broad range of orientations that average to a value of 29°.

Given the fact that the proximal F14 in SN15 behaves differently from the distant F14 in statherin, the conclusion that we are clearly drawn to is that proximity to the surface can greatly alter the potential energy landscape of phenylalanine side chains. This is affirmed by observations of gas-phase phenylalanine residues adsorbed on to various metallic surfaces,[53] where under conditions of strong binding the phenylalanine residues prefer nonstatistical conformations to maximize electronic overlapping.

Comparison of Phenylalanine Dynamics in Surface-Bound and Solution States. There is an observed correspondence between the results derived near the surface (both in the current manuscript and in the RosettaSurface.NMR study) and those observed for phenylalanine side chains in solution-state NMR studies of the decapeptide antamanide (Bremi et al).[40] The distributions of the χ_1 dihedral angle exemplify this similarity well. Bremi et al. discuss two different types of phenylalanine residues: one with a single peak in the χ_1 landscape, and one with three peaks. The residue with a single peak prefers a conformation with a χ_1 angle near −60° (or ∼300° using the conventions of our analysis here), whereas

dx.doi.org/10.1021/ja504677d | J. Am. Chem. Soc. 2014, 136, 11402−11411

the residue with three peaks exchanges between χ_1 orientations near {−180° to −150°}, {−90° to −60°} and 60° (or {180° to 210°}, {270° to 300°} and 60° using our conventions).

This is similar to the cases of F7 and F14, with the RosettaSurface.NMR clustering of F7 producing two peaks, and that of F14 producing three peaks (Figure 4). The two peaks for F7 and the three peaks for F14 occur in almost exactly the same angular positions as those of the three-peak-residue in the solution-state analysis.

There are a few possible explanations for this. The correspondence seems to suggest that the restriction imposed on the phenylalanine side chains by crystal packing is removed near the surface by extrusion of the side chain into an almost solution-like state of conformational freedom. The surface may have a direct or indirect (secondary-structure-based) impact on the distribution of conformers for F7 relative to those available in solution, while allowing for the same geometry. This may entail the increase of barrier size between possible conformers, leading to two instead of three. In the F14 case, the solution-state and RosettaSurface.NMR statherin conformers agree very well, implying a great degree of conformational freedom at this site in the HAP-bound compound. However, from the results for SN15 reported in this manuscript, we see that there is some degree of constraining of the motion due to proximity of F14 to the surface in the fragment−HAP system. Thus, while weak or no binding to the surface (F7) can mimic solution conditions, stronger binding (F14) on the other hand seems to lead to an intermediate situation where the conformational flexibility is greater than that in crystal structures but less than that in solution (fewer exchange partners).

The χ_2 comparisons are a little more ambiguous: while the solution distributions indicate differences in χ_2 angles that are separated by 180° flips, the statherin structures do not follow suit. It is possible that the statherin structures have skewed flips induced by surface adsorption, or that the RosettaSurface.NMR structures represent average positions.

5. CONCLUSION

We have demonstrated that the dynamic behavior of phenylalanine rings is modified from their unbound state versus when they are bound to the HAP surface. In the unbound state, the primary determinant of the line shape and relaxation times is the π flip motion, with any further side-chain conformational exchange occurring at a rate slower than that detectable through the available experimental data. On the other hand, fitting the line shapes and relaxation times for the HAP-bound phenyl rings involved both a significantly faster π flip motion as well as an exchange between different orientations of the C_α−C_β (χ_1 dihedral angle) and C_β−C_γ (χ_2 dihedral angle) bonds. There thus appears to be an increased flexibility of the side chains of phenylalanine residues in the presence of certain surfaces. Comparisons with computer simulations show significant similarities, while simultaneously highlighting interesting differences associated with truncation effects. This is an indication of the need for a better understanding of the modification of the potential energy surfaces of protein side chains by proximal surfaces.

■ ASSOCIATED CONTENT

Supporting Information

Description of theory of simulation methods. Experimental results of unbound SN15 experiments. Experimental line shapes for F7 and F14 in SN15 bound to HAP as a function of temperature. Discussion of the results for the unbound phenylalanines. Figure S1. Experimental and simulated deuterium line shapes of F7 in unbound SN15. Figure S2. Experimental and simulated deuterium line shapes of F14 in unbound SN15. Figure S3. Experimental deuterium line shapes of F7 and F14 in SN15 bound to HAP as a function of temperature. Table S1. T_1 values for static and mobile deuterons of F7 and F14 as a function of temperature. Table S2. Simulation parameters for fits to line shape for F7 and F14 as a function of temperature. This material is available free of charge via the Internet at http://pubs.acs.org.

■ AUTHOR INFORMATION

Corresponding Author

drobny@chem.washington.edu

Notes

The authors declare no competing financial interest.

■ ACKNOWLEDGMENTS

This work was supported by National Science Foundation Grant CHE 1219509. The authors thank Prof. Jeffrey Gray and Dr. David Masica of Johns Hopkins University for providing the computational structures and for helpful discussions.

■ REFERENCES

(1) *Proteins at Interfaces III: State of the Art*; Horbett, T.; Brash, J. L.; Norde, W., Eds.; American Chemical Society: Washington, D. C., 2012.

(2) Kroger, N.; Lorenz, S.; Brunner, E.; Sumper, M. *Science* **2002**, *298*, 584−6.

(3) Masica, D. L.; Ash, J. T.; Ndao, M.; Drobny, G. P.; Gray, J. J. *Structure* **2010**, *18*, 1678−87.

(4) Masica, D. L.; Gray, J. J.; Shaw, W. J. *J. Phys. Chem. C* **2011**, *115*, 13775−13785.

(5) Ndao, M.; Ash, J. T.; Breen, N. F.; Goobes, G.; Stayton, P. S.; Drobny, G. P. *Langmuir* **2009**, *25*, 12136−43.

(6) Ndao, M.; Ash, J. T.; Stayton, P. S.; Drobny, G. P. *Surf. Sci.* **2010**, *604*, L39−L42.

(7) Weidner, T.; Breen, N. F.; Li, K.; Drobny, G. P.; Castner, D. G. *Proc. Natl. Acad. Sci. U. S. A.* **2010**, *107*, 13288−13293.

(8) Weidner, T.; Dubey, M.; Breen, N. F.; Ash, J.; Baio, J. E.; Jaye, C.; Fischer, D. A.; Drobny, G. P.; Castner, D. G. *J. Am. Chem. Soc.* **2012**, *134*, 8750−3.

(9) Makrodimitris, K.; Masica, D. L.; Kim, E. T.; Gray, J. J. *J. Am. Chem. Soc.* **2007**, *129*, 13713−13722.

(10) Gath, J.; Hoaston, G. L.; Vold, R. L.; Berthoud, R.; Coperet, C.; Grellier, M.; Sabo-Etienne, S.; Lesage, A.; Emsley, L. *Phys. Chem. Chem. Phys.* **2009**, *11*, 6962−71.

(11) Naito, A.; Iizuka, T.; Tuzi, S.; Price, W. S.; Hayamizu, K.; Saito, H. *J. Mol. Struct.* **1995**, *355*, 55−60.

(12) Batchelder, L. S.; Sullivan, C. E.; Jelinski, L. W.; Torchia, D. A. *Proc. Natl. Acad. Sci. U. S. A.* **1982**, *79*, 386−389.

(13) Allerhand, A.; Gutowsky, H. S. *J. Chem. Phys.* **1965**, *42*, 4203−4212.

(14) Smith, R. L.; Oldfield, E. *Science* **1984**, *225*, 280−8.

(15) Spiess, H. W. In *Dynamic NMR Spectroscopy*; Diehl, P., Fluck, E., Kosfeld, R., Eds.; Springer-Verlag: Berlin, 1978; Vol. *15*, pp 55−214.

(16) Wittebort, R. J.; Olejniczak, E. T.; Griffin, R. G. *J. Chem. Phys.* **1987**, *86*, 5411.

(17) Vold, R. R.; Vold, R. L. *Adv. Magn. Opt. Reson.* **1991**, *16*, 85−171.

(18) Mantsch, H. H.; Saito, H.; Smith, I. C. P. *Prog. Nucl. Magn. Reson. Spectrosc.* **1977**, *11*, 211−271.

(19) Gall, C. M.; DiVerdi, J. A.; Opella, S. J. *J. Am. Chem. Soc.* **1981**, *103*, 5039−5043.

(20) Vugmeyster, L.; Ostrovsky, D.; Penland, K.; Hoatson, G. L.; Vold, R. L. *J. Phys. Chem. B* **2013**, *117*, 1051−1061.
(21) Vugmeyster, L.; Ostrovsky, D. *J. Chem. Phys.* **2014**, *140*, 075101.
(22) Vold, R. L.; Hoatson, G. L.; Vugmeyster, L.; Ostrovsky, D.; De Castro, P. J. *Phys. Chem. Chem. Phys.* **2009**, *11*, 7008−7012.
(23) Breen, N. F.; Li, K.; Olsen, G. L.; Drobny, G. P. *J. Phys. Chem. B* **2011**, *115*, 9452−60.
(24) Breen, N. F.; Weidner, T.; Li, K.; Castner, D. G.; Drobny, G. P. *J. Am. Chem. Soc.* **2009**, *131*, 14148−9.
(25) Campbell, A. A.; Ebrahimpour, A.; Perez, L.; Smesko, S. A.; Nancollas, G. H. *Calcif. Tissue Int.* **1989**, *45*, 122−128.
(26) Jensen, J. L.; Lamkin, M. S.; Oppenheim, F. G. *J. Dent. Res.* **1992**, *71*, 1569−1576.
(27) Johnsson, M.; Richardson, C. F.; Bergey, E. J.; Levine, M. J.; Nancollas, G. H. *Arch. Oral Biol.* **1991**, *36*, 631−636.
(28) Raj, P. A.; Marcus, E.; Sukumaran, D. K. *Biopolymers* **1998**, *45*, 51−67.
(29) Schwartz, S. S.; Hay, D. I.; Schluckebier, S. K. *Calcif. Tissue Int.* **1992**, *50*, 511−517.
(30) Schlesinger, D. H.; Hay, D. I. *J. Biol. Chem.* **1977**, *252*, 1689−95.
(31) Amano, A.; Kataoka, K.; Raj, P. A.; Genco, R. J.; Shizukuishi, S. *Infect. Immun.* **1996**, *64*, 4249−4254.
(32) Ramasubbu, N.; Thomas, L. M.; Bhandary, K. K.; Levine, M. J. *Crit. Rev. Oral Biol. Med.* **1993**, *4*, 363−370.
(33) Gururaja, T. L.; Levine, M. J. *Pept. Res.* **1996**, *9*, 283−9.
(34) Raj, P. A.; Johnsson, M.; Levine, M. J.; Nancollas, G. H. *J. Biol. Chem.* **1992**, *267*, 5968−76.
(35) Shaw, W. J.; Long, J. R.; Campbell, A. A.; Stayton, P. S.; Drobny, G. P. *J. Am. Chem. Soc.* **2000**, *122*, 7118−7119.
(36) Gibson, J. M.; Popham, J. M.; Raghunathan, V.; Stayton, P. S.; Drobny, G. P. *J. Am. Chem. Soc.* **2006**, *128*, 5364−70.
(37) Shaw, W. J.; Long, J. R.; Dindot, J. L.; Campbell, A. A.; Stayton, P. S.; Drobny, G. P. *J. Am. Chem. Soc.* **2000**, *122*, 1709−1716.
(38) Goobes, G.; Goobes, R.; Shaw, W. J.; Gibson, J. M.; Long, J. R.; Raghunathan, V.; Schueler-Furman, O.; Popham, J. M.; Baker, D.; Campbell, C. T.; Stayton, P. S.; Drobny, G. P. *Magn. Reson. Chem.* **2007**, *45* (Suppl 1), S32−47.
(39) Koutsopoulos, S.; Dalas, E. *Langmuir* **2000**, *16*, 6739−6744.
(40) Bremi, T.; Bruschweiler, R.; Ernst, R. R. *J. Am. Chem. Soc.* **1997**, *119*, 4272−4284.
(41) *Solid-Phase Synthesis: A Practical Guide*; Kates, S. A.; Albericio, F., Eds.; Marcel Dekker, Inc.: New York, 2000.
(42) Duer, M. J.; Levitt, M. H. *Solid State Nucl. Magn. Reson.* **1992**, *1*, 211−215.
(43) Kristensen, J. H.; Bildsoe, H.; Jakobsen, H. J.; Nielsen, N. C. *J. Magn. Reson.* **1992**, *100*, 437−443.
(44) Dueck, G.; Scheuer, T. *J. Comput. Phys.* **1990**, *90*, 161−175.
(45) Gall, C. M.; Cross, T. A.; DiVerdi, J. A.; Opella, S. J. *Proc. Natl. Acad. Sci. U. S. A.* **1982**, *79*, 101−105.
(46) Hiraoki, T.; Kogame, A.; Nishi, N.; Tsutsumi, A. *J. Mol. Struct.* **1998**, *441*, 243−250.
(47) Kinsey, R. A.; Kintanar, A.; Oldfield, E. *J. Biol. Chem.* **1981**, *256*, 9028−9036.
(48) Shapovalov, M. V.; Dunbrack, R. L., Jr. *Structure* **2011**, *19*, 844−858.
(49) Vugmeyster, L.; Ostrovsky, D.; Ford, J. J.; Burton, S. D.; Lipton, A. S.; Hoatson, G. L.; Vold, R. L. *J. Am. Chem. Soc.* **2009**, *131*, 13651−13658.
(50) Huang, Y. Ph.D. Thesis, College of William and Mary, Williamsburg, VA, 2007.
(51) Masica, D. L.; Gray, J. J. *Biophys. J.* **2009**, *96*, 3082−91.
(52) Masica, D. L.; Schrier, S. B.; Specht, E. A.; Gray, J. J. *J. Am. Chem. Soc.* **2010**, *132*, 12252−12262.
(53) Ghiringhelli, L.; Site, L. D. *J. Am. Chem. Soc.* **2008**, *130*, 2634−2638.